Title

In vivo quantification of optical contrast agent dynamics in rat tumors by use of diffuse optical spectroscopy with magnetic resonance imaging coregistration.

Journal

Applied Optics, 42(16)

ISSN

1559-128X

Authors

Cuccia, David J

Bevilacqua, Frederic

Durkin, Anthony J

et al.

Publication Date

2003-06-01

DOI

10.1364/ao.42.002940

In vivo quantification of optical contrast agent dynamics in rat tumors by use of diffuse optical spectroscopy with magnetic resonance imaging coregistration

David J. Cuccia, Frederic Bevilacqua, Anthony J. Durkin, Sean Merritt, Bruce J. Tromberg, Gultekin Gulsen, Hon Yu, Jun Wang, and Orhan Nalcioglu

We present a study of the dynamics of optical contrast agents indocyanine green (ICG) and methylene blue (MB) in an adenocarcinoma rat tumor model. Measurements are conducted with a combined frequency-domain and steady-state optical technique that facilitates rapid measurement of tissue absorption in the 650–1000-nm spectral region. Tumors were also imaged by use of contrast-enhanced magnetic resonance imaging (MRI) and coregistered with the location of the optical probe. The absolute concentrations of contrast agent, oxyhemoglobin, deoxyhemoglobin, and water are measured simultaneously each second for approximately 10 min. The differing tissue uptake kinetics of ICG and MB in these late-stage tumors arise from differences in their effective molecular weights. ICG, because of its binding to plasma proteins, behaves as a macromolecular contrast agent with a low vascular permeability. A compartmental model describing ICG dynamics is used to quantify physiologic parameters related to capillary permeability. In contrast, MB behaves as a small-molecular-weight contrast agent that leaks rapidly from the vasculature into the extravascular, extracellular space, and is sensitive to blood flow and the arterial input function.

OCIS codes: 170.6510, 170.1470.

1. Introduction

The use of contrast agents to analyze diseased tissues is a standard diagnostic modality in medicine today. Specifically, much progress has been made in nuclear medicine and dynamic contrast-enhanced magnetic resonance imaging (DCE-MRI) toward the characterization of blood perfusion and of capillary leakage in breast and brain tumors.[1] Recent advances in the development of quantitative near-infrared (NIR) diagnostic technologies and molecular probe design have stimulated increased interest in the use of optical contrast agents for similar medical applications. Highlights of the recent advances in optical contrast agents for NIR molecular probe-based applications in medicine[2] include cancer detection,[3,4] measurement of cerebral blood flow,[5] burn depth assessment,[6] monitoring of muscle function,[7] and monitoring of photosensitizer concentration for photodynamic therapy.[8]

Optical measurement of tumor physiology at the microvessel level has a strong clinical potential for predicting and monitoring patient response to therapies. High levels of tumor perfusion have been shown to predict low tumor recurrence after radiotherapy.[9] Also, tumor vessel permeability to macromolecular blood solutes has been shown to correlate with tumor growth, metatsatic potential, and eventual therapeutic outcome.[10,11] In addition to its direct clinical applications, this technique could be useful for testing drug efficacy in animals, providing drug makers with a robust and inexpensive method for rapid evaluation of new therapeutic drugs.

Noninvasive measurement of optical contrast agent dynamics in tumors after intravenous injection has been reported previously.[3,4,8,12] Ntziachristos *et al.*[4] report coregistration of indocyanine green- (ICG-) enhanced diffuse optical tomography

D. J. Cuccia, F. Bevilacqua, A. J. Durkin, S. Merritt, and B. J. Tromberg (tromberg@laser.bli.uci.edu) are with the Laser Microbeam and Medical Program, Beckman Laser Institute, University of California Irvine, Irvine, California 92612. G. Gulsen, H. Yu, J. Wang, and O. Nalcioglu (nalci@uci.edu) are with the John Tu and Thomas Yuen Center for Functional Onco-Imaging, University of California Irvine, Irvine, California 92697-5020.

Received 6 September 2002; revised manuscript received 2 January 2003.

0003-6935/03/162940-11$15.00/0

and gadolinium-diethylenetriamine pentaacetic acid- (Gd-DTPA-) enhanced MRI in the human breast. Demonstrating ICG contrast as a potential reporter of tumor state, this study showed colocalization of Gd-DTPA and ICG image enhancement for both a ductal carcinoma and a fibroadenoma, in which both ICG and Gd-DTPA enhancements were attributed to differences in vascular density. Gurfinkel *et al*.[3] employ a pharmacokinetic model to describe the selective uptake of arotene-conjugated 2-devinyl-2-(1-hexyloxyethyl) pyropheophorbide (HPPH-car, a photosensitizer) and nonselective uptake of ICG in canine mammary tumors, measured by fluorescence techniques. For HPPH-car, fitting coefficients are shown to distinguish between tumor and normal tissue, whereas those for ICG show no statistical difference between these tissue types. However, because the pharmacokinetic model used in this analysis was underdetermined, separation of individual pharmacokinetic variables such as the rate of ICG tissue uptake was not possible, resulting in an incomplete quantitative comparison of tumor with normal tissue. Although these studies represent important advances in the analysis of optical contrast agent dynamics in tumors, to date there have not been significant reports demonstrating quantitative analysis of these dynamics in terms of tumor physiological parameters, such as capillary permeability and blood flow.

In the research discussed herein, we introduce optical contrast agents ICG and methylene blue (MB) to be used for quantitative assessment of tumor physiology. We demonstrate measurement of ICG and MB concentration dynamics after bolus dose administration *in vivo* with high spectral and temporal resolution. First, we present a method used to determine the concentration of MB and ICG *in vivo*. Second, we show ICG and MB time course results on a rat tumor model, which were simultaneously investigated with MRI. Gd-DTPA-enhanced MRI measurements are used to differentiate between necrotic and edematous tissues, and resulting NIR MB results correlate well with perfusion dynamics expected from MRI images. Finally, a compartmental model is developed for quantitatively describing the observed ICG pharmacodynamics. In a companion paper, the relationship between NIR results and MR images is further elucidated with Gd-DTPA as a MR contrast agent.[13]

2. Materials and Methods

A. Contrast Agents

The exogenous optical contrast agents used in this study were MB and ICG, with molecular weights of 373.9 Da and 775.0 Da, respectively. Both dyes are inexpensive and have been cleared by the Food and Drug Administration (FDA) for limited intravenous applications.[14,15] MB is a water-soluble small-molecular-weight contrast agent. ICG is a blood pool agent that binds to globulin proteins (predominantly albumin) in blood. ICG is removed from the circulation through active metabolism by the liver.[16] Because ICG rapidly and completely binds to albumin after injection,[4] the temporal dynamics of albumin *in vivo* govern the kinetics of ICG. Albumin is a large, negatively charged globulin protein with a high intravascular concentration of approximately 40 mg/ml, or 603.8 μM (MW = 66-κDa). Because of its albumin binding, ICG's *effective* molecular weight is 67 kDa; thus its kinetics are governed by the movement of albumin in and between the vascular compartment and the extravascular, extracellular space (EES).

B. Tumor Model

Tumor cells (R3230ac, adenocarcinoma) were injected subcutaneously into ten Fischer rats, 2–3 wk prior to measurement. All rats were managed in accordance with the Institutional Animal and Use Committees protocol 2002-2323-0. Rats ranged in weight from 170 to 210 g after 5 wk. A detailed study of the changes in tumor as evidenced by MRI and endogenous NIR chromophores over the course of 20 days was carried out, and the results of this research are reported in the companion paper by Merritt *et al*.[13] Contrast agent experiments were conducted on four of these rats just before sacrifice. Tumor sizes for these rats ranged in diameter from 5 to 30 mm. The rats were anesthetized prior to NIR and MRI interrogation.

C. Combined Frequency-Domain and Steady-State Method

Before contrast agent injection, baseline measurements of tissue optical properties were made with a combined multiwavelength frequency-domain photon migration and steady-state broadband reflectance technique (SS-FDPM) that has been recently reported in detail.[17,18] Both frequency-domain and cw measurements were performed in a reflectance geometry, each at a single source–detector separation. The frequency-domain and steady-state source–detector separations were both 5.7 mm. We analyzed this geometry with a Monte Carlo simulation (see Merritt *et al*.[13] in this issue) and found that the average depth of optical interrogation was approximately 1.8 mm. Second, we determined that the contribution of 0.5-mm epidermal layer with a reasonable range of optical properties was small. Source and detector portions of the system were completely fiber based, with specially designed nonmetallic probes to allow placement inside homebuilt small-animal coils of a 3-tesla full-body MRI magnet, shown in Fig. 1.

The optical fibers were routed through a wall into an adjacent room where the SS-FDPM instrumentation was located. Copper sulfate tubes incorporated into the probe allowed visualization by T_2-weighted MR images and thus coregistration of optical and MR data, demonstrated in Fig. 2.

Frequency-domain measurements were made with laser diodes at 674, 800, 849, 898, and 915 nm, modulated at frequencies from 50 to 601 MHz, sweeping

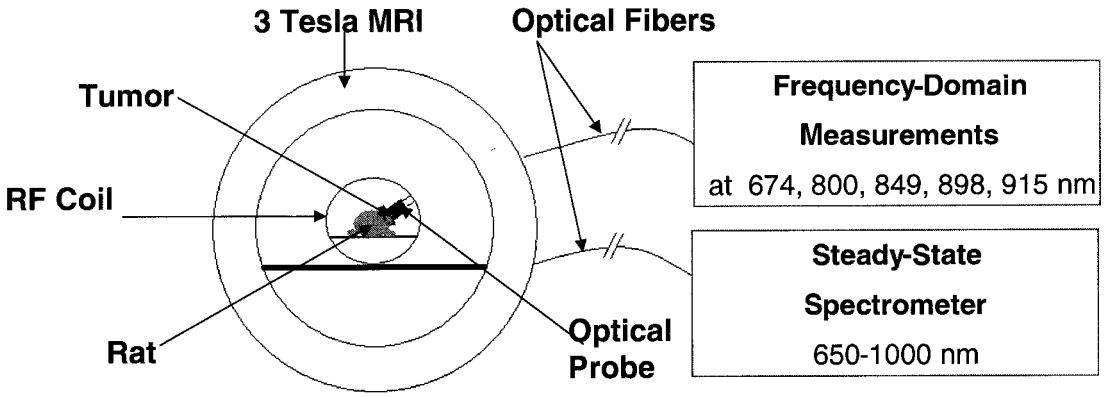

Fig. 1. SS-FDPM and MRI instrumentation diagram showing optical probe placement inside the animal coils of a 3.0-tesla magnet.

a total of 233 frequencies, and detected with an avalanche photodiode (Hamamatsu APD C556P-56045-03). Phase and amplitude data are fitted to a model of radiative transport based on the P1 approximation to the diffusion equation in order to determine the absorption (μ_a) and reduced-scattering (μ_s') coefficients at discrete wavelengths spanning the NIR. Because μ_s' follows a power-law behavior as a function of wavelength,[19] a fit to the discrete μ_s' values can be used to determine a continuous reduced-scattering spectrum from 650 to 1000 nm. In addition, a broadband cw reflectance measurement spanning the range 650–1000 nm is performed with a tungsten–halogen light source (Ocean Optics LS-1) and a spectrometer (Ocean Optics S2000; integration time, 600 ms). With the μ_s' spectrum and diffusion theory, the broadband reflectance spectra are converted to absorption coefficient spectra. Finally, we determine absolute tissue concentrations of Hb, HbO_2, and H_2O by performing a least-squares fit (Levenberg–Marquart) of the individual chromophore line shapes to the wavelength-dependent μ_a. Although our instrumentation also has the ability to determine lipid concentrations, the tumor tissues measured contained insignificant amounts of fat and did not necessitate the use of the fat spectrum in the chromophore fit.

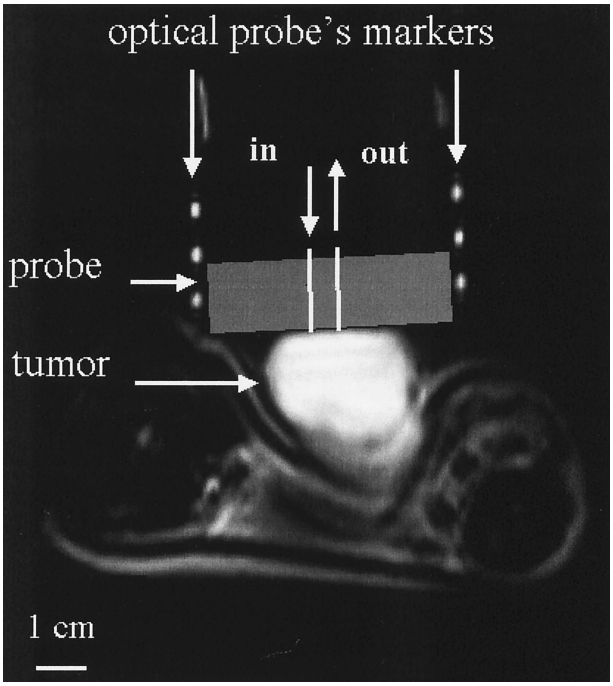

Fig. 2. T2-weighted MR image of the optical probe placement on a rat tumor. Copper sulfate tubes mark the location of the fiber probe, allowing coregistration of optical and MR data.

The capability of the system to acquire steady-state reflectance data quickly has enabled rapid (subsecond) acquisition of dynamic tissue reflectance spectra during the *in vivo* bolus passage of the contrast agents. The scattering spectrum resulting from the power-law fit to reduced-scattering (μ_s') coefficients at discrete wavelengths was determined from a SS-FDPM measurement performed prior to bolus injection and applied to each subsequent broadband reflectance spectrum acquired during the measurement time course on a particular rat. We have verified that long-term changes in tissue scattering are minimal (less than 10%), on the basis of SS-FDPM measurements made inside the MRI both before and after bolus Gd-DTPA administration. Thus, for the purposes of this study, we approximate that a bolus injection of an optical contrast agent with a saline flush does not affect the reduced tissue scattering parameter μ_s'. Finally, optical contrast agent concentrations, together with HbO_2, Hb, and H_2O, were deduced from the broadband absorption spectrum for each point in a post-bolus injection time series. This was done with multiple linear regression of the chromophore extinction coefficient spectra to each calculated absorption spectrum. MB molar extinction coefficients, measured from a 10-mM solution in H_2O, are provided by Prahl.[20] ICG molar extinction coefficients have been shown to be concentration dependent.[21] We therefore chose to use those measured by Landsman from a 6.5-μM solution in albumin,[20,21] most closely matching the blood concentration expected from the injected dose.

D. Measurement Procedure

The rats were placed inside the MRI magnet, and baseline SS-FDPM measurements were made with the probe placed normal to the tumor surface. Bolus injections of 55, 10, and 7.5 mg/kg for Gd-DTPA, MB, and ICG, respectively, were administered to the rats via the tail vein. The agents were combined with a saline flush such that the total fluid administered was 1.5 ml (≈10% of the total blood volume). The total duration of injection was approximately 1 s. Broadband reflectance measurements (acquisition rate, 1 Hz; integration time, 600 ms) were started approximately 10 s before injection and continued for approximately 10 min postinjection. The injections were performed in series with Gd-DTPA first, then MB, and finally ICG approximately 15 min after the MB injection. Gd-DTPA was injected first because it does not have an optical signature in the range 650–1000 nm. During the ICG timecourse, the contribution of the residual MB to the tissue μ_a spectrum was simultaneously fit. The entire sequence of optical measurements was performed without movement of the fiber probe to ensure reliable comparisons of data acquired from the same tissue volume.

For this study, T_1-weighted dynamic sequences and T_2-weighted images were obtained from MRI measurements. Details related to the acquisition of MRI data are can be found in a companion paper (Merritt *et al.*[13]). For a given measurement session, each rat was placed inside the rf coil and the head of the optical probe was placed on the tumor. T_2 images were acquired to locate the tumor, and the $H_2O \cdot CuSO_4$ filled markers were used to give an estimate of the location of the optical source and detector fibers relative to the tumor.

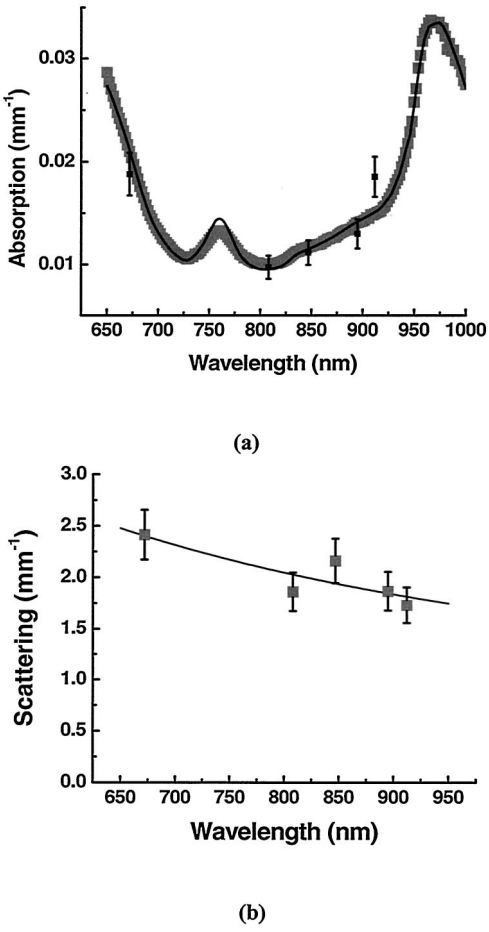

Fig. 3. (a) Preinjection frequency-domain absorption measurements (black bars), broadband absorption measurement (gray squares), and fit (black curve) versus wavelength. (b) Preinjection tissue scattering measurements (black bars) and broadband fit (black curve) versus wavelength.

3. Results and Analysis

A. SS-FDPM Measurements

Examples of tumor tissue absorption and scattering data, along with the respective broadband fits, are shown in Fig. 3, resulting from a full, preinjection SS-FDPM measurement. The magnitude of the uncertainty for both scattering and absorption is of the order of 10%. These fitting errors arise from our ability to resolve small phase shifts, a challenge posed by such short source–detector separations.

Using this preinjection fit to the spectrum of scattering coefficients in combination with postinjection broadband reflectance data and applying the diffusion approximation, we were able to deduce the broadband absorption spectrum for each time point. An example of absorption spectra both before and after (near peak concentration) injection of MB and ICG is shown in Fig. 4. Note the observed *in vivo* absorption peaks of MB and ICG at 666 and 801 nm, respectively.

B. Time-Course Data

Optical contrast agent concentrations, together with HbO_2, Hb, and H_2O, were calculated for each time point by use of multiple linear regression of chromophore extinction coefficient spectra to the calculated absorption spectrum. In Fig. 5 we show examples of time courses for both ICG and MB. Because we are quantifying a change in concentration, the error in contrast agent concentration dynamics arises from the precision of our broadband absorption measurement, approximately 2–3%, rather than from the accuracy. This is very small relative to the large 200% change in tissue absorption, yielding a measurement with high signal to noise. Note that, in the case of ICG [Fig. 5(a)] the concentration values for HbO_2, Hb, and H_2O remain approximately constant during the time course. NIR data indicate that this tumor is hypoxic, with a Hb saturation (HbO_2/[HbO_2 + Hb]) of approximately 40%. This, in combination with MR images taken of this tumor showing low levels of Gd-DTPA enhancement, suggests that this tumor was necrotic. In general we observe a 10–20% dip in HbO_2, and a 5–10% dip in Hb_{Tot}, and subsequent return to baseline over approximately 50 s following the bolus pulse. This is most likely due to a transient dilution of the arterial blood from the bolus injection, which is reasonable

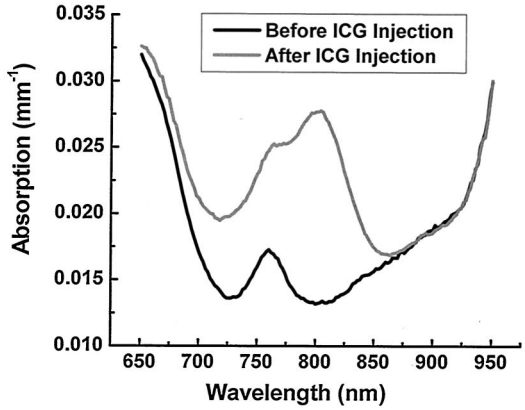

(a)

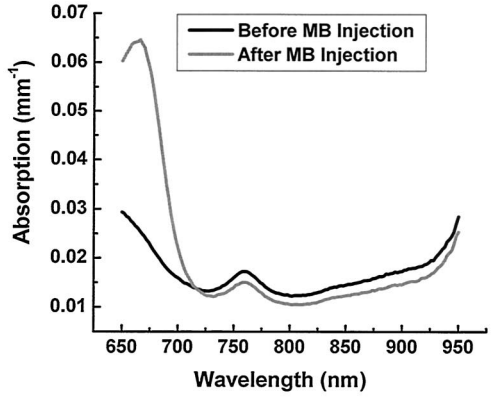

(b)

Fig. 4. (a) Pre- and postinjection absorption spectra of MB versus wavelength. (b) Pre- and postinjection absorption spectra of ICG versus wavelength.

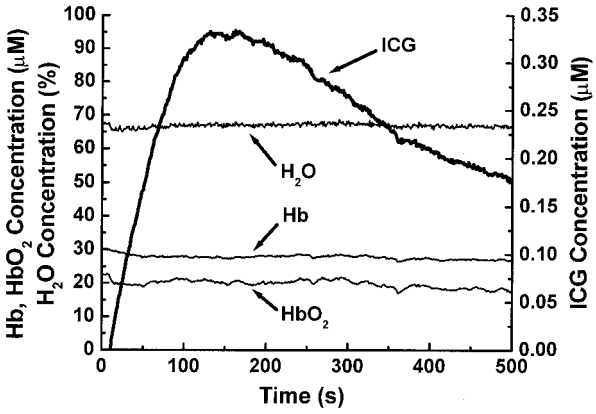

(a)

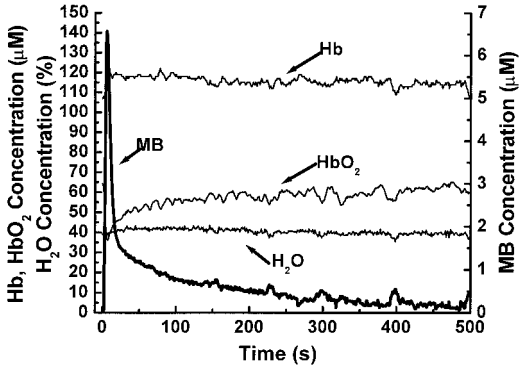

(b)

Fig. 5. (a) Absolute concentrations of Hb, HbO_2, H_2O, and contrast agent (ICG) versus time calculated with a least-squares fit to absorption coefficient as determined from the broadband component of SS-FDPM. The error bars have been removed for clarity but are typically 10%. Note that little coupling between the chromophores is observed. (b) Similar plots for MB. MB demonstrates a rapid wash-in wash-out behavior during the first pass through the circulation, whereas ICG shows a very slow tissue uptake and removal behavior.

given that the bolus injected was roughly 10% of the total blood volume.

The time courses for all four rats quickly reach a peak MB concentration and subsequently decay with an average time-to-peak and FWHM of approximately 4 and 11 s, respectively. In contrast, all tissue ICG dynamics rise and fall slowly, reaching their peak values after nearly 100 s after injection with an average FWHM of approximately 450 s. An approximate recirculation time for rats is 8 s (Ref. 22), though under anesthesia, it could be longer, owing to a slowed cardiac output. The MB dynamics appear to operate on the same time scale as the characteristic recirculation time, whereas those for ICG clearly operate on a time scale much larger than this characteristic time. Because the time dynamics of ICG and MB are very different, the signals suggest that they are governed by different physiologic phenomena.

As mentioned above, albumin-bound ICG (67 kDa) kinetics demonstrate macromolecular behavior. Under normal physiological conditions, intravascular structures larger than 60 kDa are generally restricted to the vascular space, being too large to pass through the capillary endothelial junctions. In neoplastic tissue, the presence of discontinuous capillaries is believed to make vessels hyperpermeable to macromolecular blood solutes. However, even under normal conditions, albumin is known to leak slowly to the EES at an average rate of 4–5%/h.[23] This is due to hydrostatic and osmotic gradients that produce an albumin concentration 30% higher in the EES than in the vascular compartment.

C. Methyl Blue and Indocyanine Green Pharmacokinetics

Direct interpretation of the tissue concentration curves in Fig. 5 is complex because the contrast agent concentration is an unknown combination of vascular and EES compartmental concentrations. These time-dependent concentrations are governed by the global and local blood flow as well as the permeability

of the capillary to the particular agent being considered.

Standard pharmacokinetic principles highlight the difference between the tissue uptake of small- and large-molecular-weight contrast agents such as MB and ICG, respectively. For a review of tracer kinetic models used for dynamic contrast enhanced MRI, see Tofts.[1] The effect on MR tracer dynamics by varying the molecular weight is highlighted in Su *et al*.[24] Applying these principles to our observations of MB and ICG in tumors, we observe the following:

(1) MB demonstrates characteristics of a small-molecular-weight agent, whose diffusion across the capillary membrane occurs quickly, therefore yielding time dynamics that reflect local blood flow.

(2) Albumin-bound ICG acts as a macromolecular agent whose low transcapillary permeability slows diffusion to a regime where flow-dependent vascular distribution effects are minimal, allowing simple modeling of the concentration dynamics in terms of its distribution between plasma and EES tissue compartments.

D. Methylene Blue Analysis

The example of MB kinetics in Fig. 5 demonstrates strong sensitivity to blood flow, as it clearly shows the passage of the bolus pulse. This resembles the arterial input function (AIF) or the shape of the first-pass bolus pulse measured in an artery, described by Simpson and colleagues.[25] At the *microvascular* level, postartery pulse spreading, or dispersion, occurs from navigation of the tortuous tumor microvessel structure. In fact, the bolus pulse at the tissue level can be modeled as a convolution of the AIF with the local tissue's resistance to flow.[25] For an equivalent AIF, upstream from the tumor vasculature, the spatial heterogeneity of AIF dispersion within a tumor should reflect the status of local tissue perfusion. Therefore optical measurement of the tissue-level AIF could lead to many key insights into tumor vascular resistance and vessel structure.

The tissue MB concentration versus time in Fig. 5(b) suggests rapid extravasation of the agent from the plasma compartment into the EES, as it clearly shows the bolus pulse. Here the MB concentration in the EES is close to being flow limited, such that the plasma and EES concentrations of MB equilibrate rapidly compared with the rate of MB delivery to tissue via flow. This direct visualization of the tissue-level AIF allows for interrogation of flow heterogeneity within the tumor.

The MB signal provides information related to tumor vascular state, as confirmed qualitatively by MRI. Figure 6(a) shows Gd-DTPA "fast" and "slow" enhancing regions for the tumor of Rat 2 as measured by MRI. Low levels of enhancement can indicate edema or necrosis.[10] Figure 6(b) shows a plot of MB dynamics measured over a short time scale (25 s) in Gd-DTPA fast and slow enhancing regions. As expected, the poorly enhanced tumor regions show both a significant decrease in absolute intensity of the MB

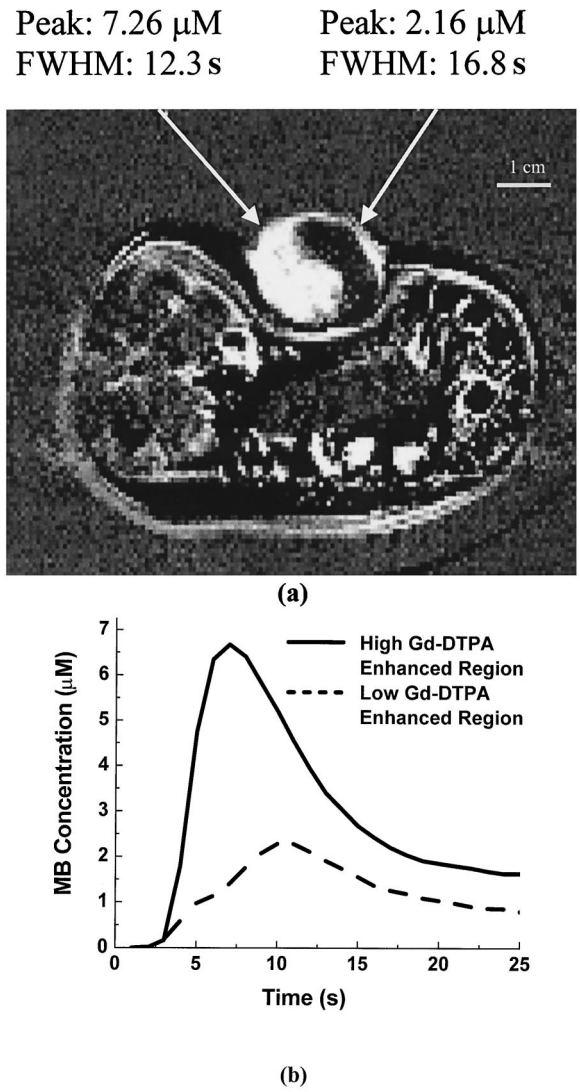

Fig. 6. (a) MRI Gd-DTPA enhancement map with MB peak information located above each region. (b) MB concentration during short times for quickly enhanced (solid curve) and slowly enhanced (dotted curve) regions of the tumor.

signal (2.16 μM versus 7.26 μM) as well as slower AIF kinetics (16.8-s FWHM versus 12.3-s FWHM). This is in agreement with the characteristics of edematous tumors, where the high intratumoral hydrostatic pressure decreases regional blood flow and therefore slows the delivery of agent to the tissue. Our NIR analysis of this tissue region in terms of endogenous chromophores (see companion paper, Merritt *et al*.[13]) confirmed that the water concentration in this case was considerably greater than that seen in normal and necrotic tissue. This optical measurement of perfusion heterogeneity could provide a new research tool for studying chemotherapeutic and photosensitizer drug delivery and a clinical tool for calibrating the dose of these drugs on an individual patient basis.

When we focus on MB dynamics over a long time scale, differing kinetic behaviors are found between

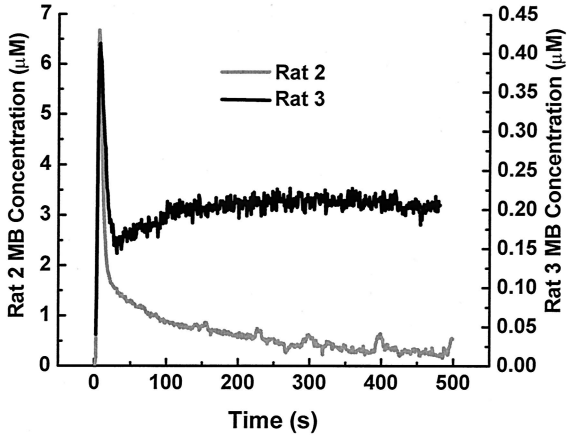

Fig. 7. MB time dynamics for two different rats. The initial pulse shapes are similar, demonstrating the bolus pulse. However the MB in Rat 2 decays away, whereas that for Rat 3 begins to rise again, displaying behavior of hindered diffusion across the capillary membrane. Second, the peak concentration of Rat 3 is much smaller than that of Rat 2, supporting the idea of hindered diffusion.

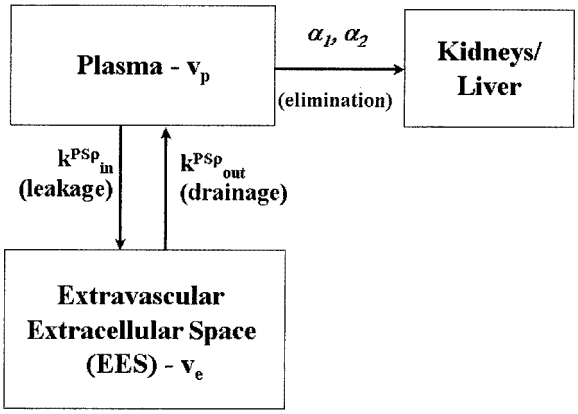

Fig. 8. Representation of the two-compartment pharmacokinetic model. v_p and v_e represent the plamas and EES compartments, respectively. $k_{in}^{PS\rho}$ and $k_{out}^{PS\rho}$ represent the leakage into and the drainage out of the EES, respectively. α_1 and α_2 are the exponents of the terms that describe the biexponential removal of ICG by metabolic processes.

different tumors. Figure 7 depicts MB time courses for two different rats (Rats 2 and 3). Whereas the MB concentration of Rat 2 continues to decay throughout the entire measurement after its peak (as was the case with three of the four rats), the MB signal of Rat 3 begins to rise again after approximately 30 s.

This is evidence that there are capillary permeability effects present, where MB diffusion into the EES is partially inhibited. In the case of Rat 3, the flow-limited assumption we have made about MB dynamics breaks down. Qualitatively, this would indicate that the Rat 3 tumor exhibits a lower permeability than the others. Also, the Rat 3 time course displays a much lower absolute MB concentration, with a peak at 0.42 μM versus 6.7 μM for Rat 2. This further supports the idea of hindered permeability, because the full amount of MB in the vasculature would never equilibrate with the large EES volume, resulting in a smaller average tissue concentration. These results are consistent with ICG fitting results presented in Subsection 3.E.

E. Indocyanine Green Compartmental Model

In tumors, increased capillary permeability allows albumin-bound molecules such as ICG to extravasate slowly into the EES.[26] To investigate this further, a simple two-compartment model was chosen to represent the plasma and EES compartment distributions, shown in Fig. 8. The leakage into and the extraction out of the EES, given by $k_{in}^{PS\rho}$ and $k_{out}^{PS\rho}$, respectively, is given by

$$\frac{dC_e}{dt} = k_{in}^{PS\rho} C_p - k_{out}^{PS\rho} C_e, \tag{1}$$

where the k's are the permeability surface-area product given by PSρ, where P is the capillary permeability constant (in centimeters per second), S is the capillary surface area (in square centimeters) per unit tissue mass, and ρ is the tissue density (in grams per cubic centimeter). The inward and outward capillary permeabilities are modeled separately to account for physiologic effects such as electric and osmotic gradients that affect albumin movement. The metabolic removal of ICG from the bulk plasma compartment can be approximated by a biexponential decay[4]:

$$C_p(t) = A_1 \exp(-\alpha_1 t) + A_2 \exp(-\alpha_2 t). \tag{2}$$

The actual bulk ICG concentration in the tissue that we measure by NIR spectroscopy, C_t, is a linear combination of the plasma concentration, C_p, and the EES concentration, C_e, with weights given directly by v_p and v_e, respectively:

$$C_t = v_p C_p + v_e C_e. \tag{3}$$

It has been shown that the plasma volume fraction, v_p, can be significantly large in tumors, requiring consideration of ICG absorption from both compartments.[1] Solving equations (1)–(3) for C_t, assuming the initial condition that $C_e(t = 0) = 0$, yields a triexponential solution:

$$\begin{aligned} C_t(t) = {} & A_1\left(v_p + \frac{v_e k_{in}^{PS\rho}}{k_{out}^{PS\rho} - \alpha_1}\right)\exp(-\alpha_1 t) + A_2\left(v_p \right. \\ & \left. + \frac{v_e k_{in}^{PS\rho}}{k_{out}^{PS\rho} - \alpha_2}\right)\exp(-\alpha_2 t) - \left[A_1\left(\frac{v_e k_{in}^{PS\rho}}{k_{out}^{PS\rho} - \alpha_1}\right)\right. \\ & \left. + A_2\left(\frac{v_e k_{in}^{PS\rho}}{k_{out}^{PS\rho} - \alpha_2}\right)\right]\exp(-k_{out}^{PS\rho} t). \end{aligned} \tag{4}$$

This derivation is valid for $1/\alpha$ and $1/k$ time constants much longer than the recirculation time of blood contents through the circulatory system, where the initial plasma distribution effects from the bolus pulse can be ignored. Note that a least-squares fit to

this triple-exponential equation would yield six numerical values corresponding to the prefactors and exponent coefficients of each term, but there are actually eight variables for which to solve. A similar problem was encountered by Gurfinkel *et al.*[3] preventing the extraction of physiologically relevant parameters. Because v_e and k_1 always occur as a product in the representation of C_t, they can be combined to reduce the number of fitting parameters to 7. In Subsection 3.F we demonstrate a method to further constrain C_t by calculating v_p directly from our optical measurements of total hemoglobin concentration. As a result, this approach allows independent quantification of $k_{\text{out}}^{\text{PS}\rho}$, v_p, $k_{\text{in}V_e}^{\text{PS}\rho}$, A_1, A_2, α_1, and α_2.

This pharmacokinetic representation differs from others proposed for ICG in that we consider transcapillary leakage to occur only at a tumor site, a small perturbation of the global plasma concentration that is not expected to affect the bulk removal [Eq. (2)] by the liver. Other biological phenomena such as bruising and sepsis, which also elevate transcapillary permeability, would affect the validity of this assumption.[3]

F. Calculation of the Plasma Volume Fraction, v_p

Calculating v_p is useful in that it allows us to constrain the ICG pharmacokinetic model permitting calculation of the remaining physiological parameters. Calculation of the plasma volume fraction, v_p from total hemoglobin, Hb_T, is possible if the hematocrit, Hct, and the Hb concentration in the red blood cells, Hb_B, are known:

$$v_p = \left(\frac{\text{Hb}_T}{\text{Hb}_B}\right)\left(\frac{100 - \text{Hct}}{\text{Hct}}\right) \approx 2.415 \times 10^{-4} \times \text{Hb}_T(\mu M). \quad (5)$$

Our combined frequency-domain and steady-state NIR spectroscopy measurement allows absolute quantification of Hb_T. Typical values of Hb_B and Hct are 5421 μM (34g/dl) and 44, respectively, and are relatively stable for a particular tissue type.[10] Because it correlates with vascular density, calculation of v_p also facilitates study of angiogenesis and allows comparison with those values calculated by DCE-MRI.

G. Indocyanine Green Analysis

Figure 9 shows time courses for ICG in all four rat tumors. Note that the absolute intensities as well as the time dynamics vary markedly between each rat tumor. Both the rising slope, which correlates with the permeability value (steep slope correlates with high permeability), and the peak concentrations (most sensitive to vascular volume and permeability), are of interest when related to the tumor state. Through a combination of optical measurements of H_2O and Hb_{tot} and MR images we have classified tumors as either edematous or necrotic (see companion paper, Merritt *et al.*[13]). Tumors measured on Rats 1 and 3 are believed to be necrotic, because of their low tissue hemoglobin oxygen (S_tO_2), low total Hb, and low Gd-DTPA enhancement levels. Conversely, tumors on Rats 2 and 4 exhibit edema, having a very high water content in combination with strong T_2 intensities. These results correlate with the absolute ICG intensity, where the edematous tissues demonstrate high peak values and fast-rising slopes, whereas the necrotic tissues display low peak values and slow-rising slopes.

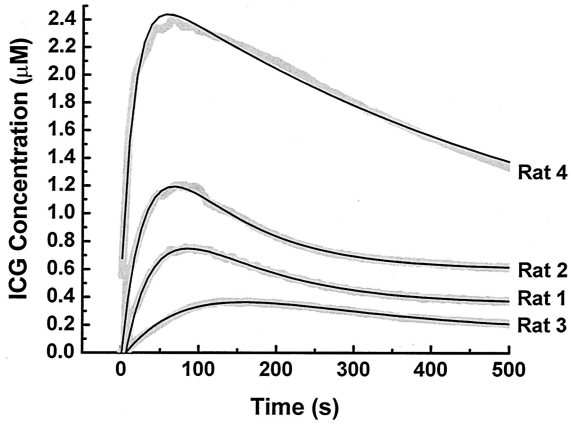

Fig. 9. Plot of ICG concentration versus time (points) and the corresponding pharmacokinetic fit (solid curve).

To characterize such differences quantitatively, the four ICG time courses in Fig. 9 were fitted to Eq. (4). Fitting was performed with a nonlinear least-squares (Levenberg–Marquart) fitting algorithm using Origin software (OriginLab Corporation, version 6.0). Calculated fitting parameters for each tumor measurement are provided in Table 1. Because of the long-term elimination of ICG from the blood is of the order of hours,[12,16] the coefficient α_1 was forced to be zero, therefore reducing the number of free parameters to five. Note that the final column of data in Table 1, v_p, is not fitted but calculated directly from measurement of total hemoglobin, Hb_T. Blood volume fractions, v_p, range from 1.26% (Rat 3) to 6.71% (Rat 4)

Table 1. Extracted Pharmacokinetic Parameters from ICG Curve Fitting

Rat Number	$k_{\text{out}}^{\text{ps}\rho}$ (sec^{-1} 10^{-2})	$k_{\text{in}V_e}^{\text{ps}\rho}$ (sec^{-1} 10^{-2})	α_2 (sec^{-1} 10^{-3})	$A_1 + A_2$ (μM)	V_p (10^{-2})
1	2.61 ± 0.02	0.58 ± 0.14	8.29 ± 0.07	4.70 ± 0.07	1.51 ± 0.02
2	3.30 ± 0.01	11.9 ± 0.1	9.45 ± 0.04	4.25 ± 0.02	4.41 ± 0.02
3	0.75 ± 0.20	11.3 ± 2.2	8.7 ± 2.1	0.61 ± 0.09	1.26 ± 0.01
4	6.10 ± 0.27	82 ± 48	1.75 ± 0.05	1.9 ± 0.9	6.71 ± 0.08

Table 2. Qualitative Summary of Results from MRI, DOS, MB and ICG

Rat No.	Tumor State	MRI	DOS	MB	ICG
1	Necrotic	Slow enhancement	Low S_tO_2	Rapid extravasation into EES	Low peak concentration; low permeability
2	Edematous	Slow enhancement; high T_2 image	High H_2O	Rapid extravasation into EES	High peak concentration; high permeability
3	Necrotic	Slow enhancement	Low S_tO_2	Hindered permeability effects (low k)	Low peak concentration; low permeability
4	Edematous	Slow enhancement; high T_2 image	High H_2O	Rapid extravasation into EES	High peak concentration; high permeability

values that are reasonable, agreeing with a level of 4–6% as reported in the literature.[27,28]

The data provide good fits to Eq. (4), and all values are physiologically reasonable and consistent between the four animals. Fitting results for $k_{\text{out}}^{\text{PS}\rho}$ range from 0.75×10^{-2} s^{-1} in Rat 2 to 6.10×10^{-2} s^{-1} in Rat 4. Average values for $k_{\text{in}}^{\text{PS}\rho}$ of an albumin-bound molecule (albumin-Gd-DTPA, 70–90 kDa) in infiltrating ductal carcinoma and fibroadenoma tumor models were determined to be $0.50 \pm 0.15 \times 10^{-2}$ s^{-1} and $0.22 \pm 0.06 \times 10^{-2}$ s^{-1}, respectively, calculated with DCE-MRI.[26] These values are generally lower than those calculated here for ICG in adenocarcinoma tumors. This is reasonable because, as mentioned above, our tumors display high levels of edema or necrosis, which would result in damaged tissue and thus increased permeability.

Confirming the qualitative analysis made at the start of this subsection, the calculated values of permeability and vascular volume correlate with the tumor state. In the necrotic tumors (Rats 1 and 3) the values of $k_{\text{out}}^{\text{PS}\rho}$ are 2.61 s^{-1} 10^{-1} and 0.75 s^{-1} 10^{-1} versus higher values of 3.30 s^{-1} 10^{-1} and 6.50 s^{-1} 10^{-1} for the edematous cases. Similarly, the v_p for the necrotic tissues are 1.51% and 1.26%, versus higher values of 4.41% and 6.71% for the edematous cases.

Also of interest from the extracted parameters is the value of $A_1 + A_2$, as this quantity represents the concentration of ICG *in the plasma* at $t = 0$, disregarding flow effects from the arterial input. Whereas the measured peak concentration in Rat 2 averaged over all the sampled tissue was only 1.20 μM, the peak concentration in the plasma was calculated to be 4.25 μM. This value, normally inaccessible through conventional tissue spectroscopy methods, provides predictive power to determine the peak concentration of *any* injected drug that is expected to flow into the tumor microvasculature. This measurement is important in that it allows comparison of the blood concentration with that actually delivered to the tissue. This measure of drug delivery to local tissue in combination with characterization of microvessel permeability could together provide clinicians with a direct measure of a patient's appropriate chemotherapeutic dose and probable response to treatment.

Under healthy tissue conditions, ICG binding to albumin in the plasma would prohibit leakage from the plasma into the EES.[3,5] However, under diseased conditions such as those found in proliferating tumors, the capillary permeability of a macromolecular contrast agent such as ICG-albumin can be much higher than normal, owing to increased leakiness of the vasculature.[24] This provides a potential means of contrast between normal and cancerous tissues.[4,21] Although the number of tabulated data is small, it is demonstrated here that extraction of transcapillary leakage rates is possible, given that the model function correctly describes ICG's compartmental distribution and elimination.

In the analysis of ICG time-course data, we have assumed a simplistic pharmacokinetic model for this preliminary analysis. Assumptions in the model have included flow-independent intercompartmental distribution of contrast agent and the ability to fit the true capillary permeability. Flow effects, particularly the initial AIF, can play a strong role in calculating accurate pharmacokinetic parameters.[7,28] Current DCE-MRI techniques often employ the AIF to correct their models for a nonhomogeneous distribution of contrast agent in the blood vessels at early times after injection.[7] The same techniques would apply toward more accurately modeling tissue compartment concentrations of ICG in the early distribution phase. For example, MB dynamic properties, which were shown to be strongly correlated with the AIF function, could be used for correcting the ICG curve, upon further validation of MB flow sensitivity.

A qualitative summary of the results obtained from MRI, diffuse optical spectroscopy (DOS), MB, and ICG data is presented in Table 2. Overall, tumor state (determined with combined MRI and DOS information) shows a correlation with optical contrast agent data. Specifically, edematous tumor tissues (Rats 2 and 4) demonstrate high capillary permeability, assessed from both the rapid extravasation of MB and high $k^{\text{PS}\rho}$ values calculated from the ICG pharmacokinetic fit. Necrotic tissues (Rats 1 and 3), demonstrate low permeability from the ICG fit, which is further supported through evidence of hindered permeability of MB.

Caution should be employed in generalizing the results obtained here to other tumor types. One should note that the results depicted here may be specific to the type of tumor investigated and/or tu-

mor state. These four tumors displayed significant signs of edema and necrosis. We hesitate to encourage broad generalization of the observed MB and ICG kinetics without investigation of other tumor types and measurements performed over the course of progression of disease. To this end, we are currently conducting a larger study that will illuminate contrast agent dynamics over the life of the tumor. However, it is clear that within the context of series of investigations, the different molecular weights of these optical contrast agents consistently yield signals that are sensitive to different physiological phenomena and that they can be modeled with existing pharmacokinetic models developed by researchers in nuclear medicine and MRI.

4. Conclusion

In conclusion, noninvasive measurement of optical contrast agent kinetics has been demonstrated by use of a combined steady-state and frequency-domain optical technique that quantifies the tissue absorption and scattering properties across the near-infrared (NIR) range of 650–1000 nm, thus allowing absolute measurement of optical contrast agent, Hb, HbO_2, and H_2O time-dependent concentrations. In four late-stage adenocarcinoma tumors, methylene blue (MB) behaves as a small-molecular-weight agent, leaking quickly from the tumor vasculature and possibly allowing visualization of the arterial input function. Local tissue pulse spreading of the MB arterial input is linked to tissue status as reflected by DCE-MRI enhancement levels, demonstrating optical sensitivity to tumor flow heterogeneity. This suggests that the MB curve may prove to be useful in quantifying local tissue perfusion, which will be examined more rigorously in a future study. Once injected, indocyanine green (ICG) binds to albumin and thus demonstrates macromolecular behavior. This results in a slow leakage that allows application of a pharmacokinetic model that, along with additional constraints provided from measurement of total hemoglobin (HbT), allows for the determination of individual vascular parameters, such as capillary permeability and blood volume fractions. The selection of differing molecular weight contrast agents, therefore, is shown to yield sensitivity to different tissue compartments and thus different physiological parameters, allowing for selective sensitivity between permeability and flow.

This study is a first step toward the use of optical contrast agents for interrogation of tumor physiology, laying the foundation for future research. One should note that these results might be specific to the type of tumor investigated and/or tumor state. The next step will be to conduct a larger study, examining how differing molecular weight contrast agent dynamics vary as a function of tumor type and stage of growth. The dynamics of Gd-DTPA will be measured by use of MRI and compared directly with time courses of optical contrast agents. Eventually, a longitudinal study will be conducted to examine change in optical tracer kinetics over the course of chemotherapy.

This study was supported by the National Institutes of Health under grants RR01192 (Laser Microbeam and Medical Program, LAMMP) and NIH P20-CA86182; the Avon Foundation; the Chao Family Comprehensive Cancer Center; and the Air Force Office of Scientific Research (AFOSR, MFEL grant #F49620-00-1-0371). A. Durkin acknowledges Michael Berns and the Beckman Foundation for fellowship support.

References

1. P. S. Tofts, "Modeling tracer kinetics in dynamic Gd-DTPA MR imaging," J. Magn. Reson. Imag. **7,** 91–101 (1997).
2. D. J. Bornhop, C. H. Contag, K. Licha, and C. J. Murphy, "Advance in contrast agents, reporters, and detection," J. Biomed. Opt. **6,** 106–110 (2001).
3. M. Gurfinkel, A. B. Thompson, W. Ralston, T. L. Troy, A. L. Moore, T. A. Moore, J. D. Gust, D. Tatman, J. S. Reynolds, B. Muggenburg, K. Nikula, R. Pandey, R. H. Mayer, D. J. Hawrysz, and E. M. Sevick-Muraca, "Pharmacokinetics of ICG and HPPH-car for the detection of normal and tumor tissue using fluorescence, near-infrared reflectance imaging: a case study," Photochem. Photobiol. **72,** 94–102 (2000).
4. V. Ntziachristos, A. G. Yodh, M. Schnall, and B. Chance, "Concurrent MRI and diffuse optical tomography of breast after indocyanine green enhancement," Proc. Natl. Acad. Sci. USA **97,** 2767–2772 (2000).
5. R. Springett, Y. Sakata, and D. T. Delpy, "Precise measurement of cerebral blood flow in newborn piglets from the bolus passage of indocyanine green," Phys. Med. Biol. **46,** 2209–2225 (2001).
6. J. M. Still, E. J. Law, K. G. Klavuhn, T. C. Island, and J. Z. Holtz, "Diagnosis of burn depth using laser-induced indocyanine green fluorescence: a preliminary clinical trial," Burns **27,** 364–371 (2001).
7. H. B. Larsson, T. Fritz-Hansen, E. Rostrup, L. Sondergaard, P. Ring, and O. Henriksen, "Myocardial perfusion modeling using MRI," Magn. Reson. Med. **35,** 716–726 (1996).
8. R. A. Weersink, J. E. Hayward, K. R. Diamond, and M. S. Patterson, "Accuracy of noninvasive *in vivo* measurements of photosensitizer uptake based on a diffusion model of reflectance spectroscopy," Photochem. Photobiol. **66,** 326–335 (1997).
9. J. Griebel, N. A. Mayr, A. de Vries, M. V. Knopp, T. Gneiting, C. Kremser, M. Essig, H. Hawighorst, P. H. Lukas, and W. T. Yuh, "Assessment of tumor microcirculation: a new role of dynamic contrast MR imaging," J. Magn. Reson. Imag. **7**(1), 111–119 (1997).
10. M. Y. Su, J. C. Jao, and O. Nalcioglu, "Measurement of vascular volume fraction and blood-tissue permeability constants with a pharmacokinetic model: studies in rat muscle tumors with dynamic Gd-DTPA enhanced MRI," Magn. Reson. Med. **32,** 714–724 (1994).
11. R. K. Jain, "Transport of molecules across tumor vasculature," Cancer Metastasis Rev. **6,** 559–593 (1987).
12. K. Licha, B. Riefke, V. Ntziachristos, A. Becker, B. Chance, and W. Semmler, "Hydrophilic cyanine dyes as contrast agents for near-infrared tumor imaging: synthesis, photophysical properties and spectroscopic *in vivo* characterization," Photochem. Photobiol. **72,** 392–398 (2000).
13. S. Merritt, F. Bevilacqua, A. J. Durkin, D. J. Cuccia, R. Lanning, B. J. Tromberg, G. Gulsen, H. Yu, J. Wang, and O. Nalcioglu, "Monitoring tumor physiology using near-infrared

spectroscopy and MRI coregistration," Appl. Opt. **42,** 2951–2959 (2003).
14. J. Fishbaugh, "Retina: indocyanine green (ICG) angiography," Insight **19**(3), 30–32 (1994).
15. L. A. Geddes, "Cardiac output measurement," in *The Biomedical Engineering Handbook* (CRC Press, Boca Raton, Fla., 1995), pp. 1212–1213.
16. M. S. Yates, C. J. Bowmer, and J. Emmerson, "The plasma clearance of indocyanine green in rats with acute renal failure: effect of dose and route of administration," Biochem. Pharmacol. **32,** 3109–3114 (1983).
17. F. Bevilacqua, A. J. Berger, A. E. Cerussi, D. Jakubowski, and B. J. Tromberg, "Broadband absorption spectroscopy in turbid media by combined frequency-domain and steady-state methods," Appl. Opt. **39,** 6498–6507 (2000).
18. D. J. Jakubowski, "Development of broadband quantitative tissue optical spectroscopy for the non-invasive characterization of breast disease," (Beckman Laser Institute, University of California, Irvine, Irvine, Calif., 2002).
19. R. Graaff, J. G. Aarnoudse, J. R. Zijp, P. M. A. Sloot, F. F. M. de Mul, J. Greve, and H. M. Koelink, "Reduced light-scattering properties for mixtures of spherical particles: a simple approximation derived from Mie calculations," Appl. Opt. **31,** 1370–1376 (1992).
20. S. Prahl, "Tabulated molar extinction coefficient for methylene blue in water," (1998), http://omlc.ogi.edu/spectra/mb/mb-water.html.
21. M. L. Landsman, G. Kwant, G. A. Mook, and W. G. Zijlstra, "Light-absorbing properties, stability, and spectral stabilization of indocyanine green," J. Appl. Physiol. **40,** 575–583 (1976).
22. M. K. Pugsley, V. Kalra, and S. Froebel-Wilson, "Protamine is a low molecular weight polycationic amine that produces actions on cardiac muscle," Life Sci. **72**(3), 293–305 (2002).
23. J. F. Payen, J. P. Vuillez, B. Geoffray, J. L. Lafond, M. Comet, P. Stieglitz, and C. Jacquot, "Effects of preoperative intentional hemodilution on the extravasation rate of albumin and fluid," Crit. Care Med. **25,** 243–248 (1997).
24. M. Y. Su, A. Muhler, X. Lao, and O. Nalcioglu, "Tumor characterization with dynamic contrast-enhanced MRI using MR contrast agents of various molecular weights," Magn. Reson. Med. **39,** 259–269 (1998).
25. N. E. Simpson, Z. He, and J. L. Evelhoch, "Deuterium NMR tissue perfusion measurements using the tracer uptake approach: I. Optimization of methods," Magn. Reson. Med. **42**(1), 42–52 (1999).
26. M. Y. Su, Z. Wang, P. M. Carpenter, X. Lao, A. Muhler, and O. Nalcioglu, "Characterization of N-ethyl-N-nitrosourea-induced malignant and benign breast tumors in rats by using three MR contrast agents," J. Magn. Reson. Imag. **9,** 177–186 (1999).
27. J. B. Fishkin, O. Coquoz, E. Anderson, M. Brenner, and B. J. Tromberg, "Frequency-domain photon migration measurements of normal and malignant tissue optical properties in a human subject," Appl. Opt. **36,** 10–20 (1997).
28. D. L. Buckley, "Uncertainty in the analysis of tracer kinetics using dynamic contrast-enhanced T1-weighted MRI," Magn. Reson. Med. **47,** 601–606 (2002).